https://doi.org/10.5194/egusphere-2026-5963
Preprint. Discussion started: 3 November 2026
© Author(s) 2026. CC BY 4.0 License.

U-DEM: High spatiotemporal resolution surface elevations of the Canadian Arctic

Ann-Sofie P. Zinck[1,*], Jonathan Ortved Melcher[1], Laura Thomson[2], and Dorthe Dahl-Jensen[1,3]

[1]Niels Bohr Institute, University of Copenhagen, Copenhagen, Denmark
[2]Department of Geography and Planning, Queen's University, Kingston, ON, Canada
[3]Centre for Earth Observation Science, University of Manitoba, Winnipeg, MB, Canada
[*]Now at: Geological Survey of Denmark and Greenland, Copenhagen, Denmark

Correspondence: Ann-Sofie P. Zinck (ansop@geus.dk)

Abstract. High-resolution glacier elevation observations are essential for resolving rapid changes in glacier geometry, but existing satellite datasets face a trade-off between spatial and temporal resolution. Here, we present U-DEM, a machine-learned glacier elevation time series that combines complementary satellite datasets to provide surface elevations at 100 m spatial and 3-month temporal resolution. We apply the approach to glaciers and ice caps of the Canadian Arctic from 2014 to 2024. High-resolution glacier elevation patterns are learned from ArcticDEM strips and reconstructed through time using CryoSat-2 elevations and Sentinel-1 backscatter as temporally repeated inputs.

Validation of U-DEM against independent ICESat-2 laser altimetry observations yields a root-mean-square error (RMSE) of 10.01 m, approximately 65% lower than the underlying CryoSat-2 elevations, with improvements across all 15 study regions, including regions not represented during training. Comparing U-DEM with kinematic Global Navigation Satellite System (GNSS) measurements on the narrow White Glacier yields RMSE values of 1.70–3.35 m, comparable to those of the ArcticDEM strips. Application examples further demonstrate the potential of U-DEM for resolving glacier elevation changes across different spatial scales. Firstly, U-DEM resolves the migration of the dynamic balance line during the ongoing surge of Chapman Glacier. Secondly, U-DEM captures localized elevation variability associated with several active subglacial lakes that is poorly resolved by CryoSat-2.

U-DEM thus demonstrates how machine learning can integrate satellite observations with complementary sampling characteristics to bridge the spatial–temporal resolution gap of individual sensors. The approach provides a framework for generating spatially detailed and temporally continuous records of glacier surface evolution from existing and future Earth observation missions.

1 Introduction

Glacier surface elevation is a fundamental measure of glacier state and change, reflecting the combined effects of surface mass balance, ice dynamics, basal processes, and changes at glacier termini. Repeated elevation observations are therefore widely used to derive glacier mass change, investigate spatial patterns of thinning and thickening, constrain and evaluate glacier models, and study dynamic processes ranging from glacier retreat and acceleration to surging and subglacial hydrological

https://doi.org/10.5194/egusphere-2026-5963
Preprint. Discussion started: 3 November 2026
© Author(s) 2026. CC BY 4.0 License.

activity (e.g., Hugonnet et al., 2021; Liang et al., 2022; Beraud et al., 2025). Resolving these processes requires observations at both sufficient spatial and temporal resolution. High spatial resolution is needed to capture localized elevation changes and complex patterns of ice redistribution, while frequent observations are required to track their evolution through time. This is particularly important for rapidly evolving phenomena such as glacier surges, where substantial volumes of ice can be redistributed over relatively short periods (e.g., Lauzon et al., 2023; Copland et al., 2024; Beraud et al., 2025; Van Wychen et al., 2025), and active subglacial lakes, where drainage and refilling produce localized and potentially short-lived changes in surface elevation (e.g., Liang et al., 2022; Zheng et al., 2026). Datasets combining high spatial and temporal resolution can therefore provide new opportunities to investigate glacier evolution and dynamic processes that may be difficult to resolve from spatially detailed but temporally sparse observations, or from frequent observations with coarse spatial resolution.

Currently, digital elevation models (DEMs) of glaciers are subject to a fundamental remote-sensing trade-off: observations with high spatial resolution typically have limited temporal coverage, whereas observations with high temporal resolution are generally spatially coarse. ArcticDEM strips provide metre-scale elevation information and can resolve fine spatial patterns in glacier surface morphology, but their temporal coverage is irregular because they depend on suitable optical stereo imagery, and individual strips may be affected by clouds, illumination conditions, and co-registration errors. ArcticDEM strips, and their Antarctic counterpart (Reference Elevation Model of Antarctica strips), have been used to study various processes at high spatial resolution such as ice melanges (Xia et al., 2025), subglacial lake drainage (Zheng et al., 2026), and ice shelf basal melting (Zinck et al., 2026). In contrast, CryoSat-2 radar altimetry provides repeated observations that are independent of daylight and cloud cover, and offer glacier DEMs on monthly resolutions when processed in swath mode (Gourmelen et al., 2018; Haacker et al., 2024). However, CryoSat-2 observations remain relatively coarse ($\sim$ 500-1000 m) compared with optical DEMs and may not resolve narrow outlet glaciers or other surface depression features surrounded by higher terrain (Zinck et al., 2026), as CryoSat-2 measures the surface closest to the satellite. Finally, because CryoSat-2 uses radar altimetry it means that it may penetrate into the snowpack and thereby not always measure the actual surface of a glacier (Slater et al., 2019). This penetration depth can have seasonal variations as dry snow allows the radar signal to penetrate deeper than wet snow, which may reflect at the surface (Slater et al., 2019). The high temporal resolution of CryoSat-2 has allowed for temporal insights into e.g., ice shelf basal melting (Davison et al., 2023), glacier mass loss caused by atmospheric-rivers-driven foehn events (Haacker et al., 2024), and variability in runoff from the Greenland Ice Sheet (Slater et al., 2021). The complementary characteristics of ArcticDEM and CryoSat-2 motivate approaches that combine information from both sensors to overcome the limitations of each individual dataset.

Several studies have demonstrated how deep learning can bridge the gap between observations with high spatial and temporal resolution, enabling the reconstruction of cryospheric variables at high spatiotemporal resolutions. Examples include sea ice concentration (Radhakrishnan et al., 2021), surface melt (de Roda Husman et al., 2024), and snow and ice temperatures (Cheng et al., 2023). Convolutional neural networks are particularly well suited for this task because they can learn spatial patterns from gridded geophysical data while simultaneously integrating information from multiple input channels. U-Net architectures, originally developed for biomedical image segmentation (Ronneberger et al., 2015), are especially effective for image-to-image prediction problems. Their encoder–decoder structure captures both large-scale context and local spatial detail through the

https://doi.org/10.5194/egusphere-2026-5963
Preprint. Discussion started: 3 November 2026
© Author(s) 2026. CC BY 4.0 License.

use of skip connections. The encoder progressively extracts increasingly abstract spatial features while reducing the spatial dimensions of the input through successive convolution and pooling operations. The decoder then reconstructs the target image at the original resolution by upsampling these learned feature representations. Skip connections transfer high-resolution feature information from the encoder to corresponding decoder layers, helping to preserve fine-scale spatial detail that may otherwise be lost during resolution coarsening. Since its introduction, numerous extensions of the original U-Net architecture have been proposed. A widely used extension is the Attention U-Net (Oktay et al., 2018), which incorporates attention gates that allow the network to focus on important spatial features while suppressing less relevant regions.

Here, we present U-DEM, a machine-learned glacier DEM time series with high spatial and temporal resolution. U-DEM combines the high spatial resolution of the ArcticDEM strips, the high temporal resolution of CryoSat-2, and the relatively high spatiotemporal resolution of Sentinel-1 to produce glacier elevation estimates at 100 m spatial and 3-month temporal resolution. Sentinel-1 is a C-band synthetic aperture radar (SAR) mission that provides spatially continuous backscatter observations largely independent of cloud cover and daylight. We hypothesize that Sentinel-1 backscatter patterns contain information on glacier surface morphology, roughness, crevassing, and melt features that is correlated with local elevation variability and therefore complements the coarser CryoSat-2 observations. Specifically, we train an Attention U-Net to learn the relationship between seasonal CryoSat-2 elevations, Sentinel-1 backscatter patterns, and ArcticDEM strip elevations. U-DEM is therefore designed to retain the temporal continuity provided by radar altimetry while recovering fine-scale spatial patterns associated with glacier topography and surface structure. We apply U-DEM to the glaciers and ice caps of the Canadian Arctic for the period 2014-2024 (Fig. 1).

The Canadian Arctic contains one of the largest glacierized regions outside the ice sheets (Pfeffer et al., 2014) and has in the last decade experienced a mass loss of more than 50 Gt yr^{-1} (Dussaillant et al., 2025). At the same time, the region hosts numerous dynamically active glaciers, including surge-type glaciers (Lauzon et al., 2023; Copland et al., 2024; Van Wychen et al., 2025), rapidly retreating marine-terminating glaciers (Cook et al., 2019), and active subglacial lake systems (Zheng et al., 2026). These processes can produce strong elevation-change signals over months to years and over spatial scales ranging from a few hundred meters to entire ice caps. Despite its importance, the Canadian Arctic has a more limited observational record than regions such as Greenland, Antarctica, and the European Alps because of the region's remoteness, limited field access, sparse in-situ observations, and the frequent cloud cover and low-level fog that limit optical satellite observations (Williamson et al., 2020). The combination of rapid change, complex dynamics, and poorly constrained bed topography makes the Canadian Arctic a particularly relevant target for high spatiotemporal resolution elevation mapping.

The remainder of this paper is structured as follows. First, we describe the input and validation datasets and their preprocessing, followed by the U-DEM methodology and model training. We then evaluate U-DEM against independent satellite and in-situ elevation measurements before demonstrating its capabilities and limitations through applications to glacier surges and subglacial lake drainage in the Canadian Arctic. Finally, we discuss the performance, applications, limitations, and future potential of U-DEM for investigating glacier elevation change and dynamics.

https://doi.org/10.5194/egusphere-2026-5963
Preprint. Discussion started: 3 November 2026
© Author(s) 2026. CC BY 4.0 License.

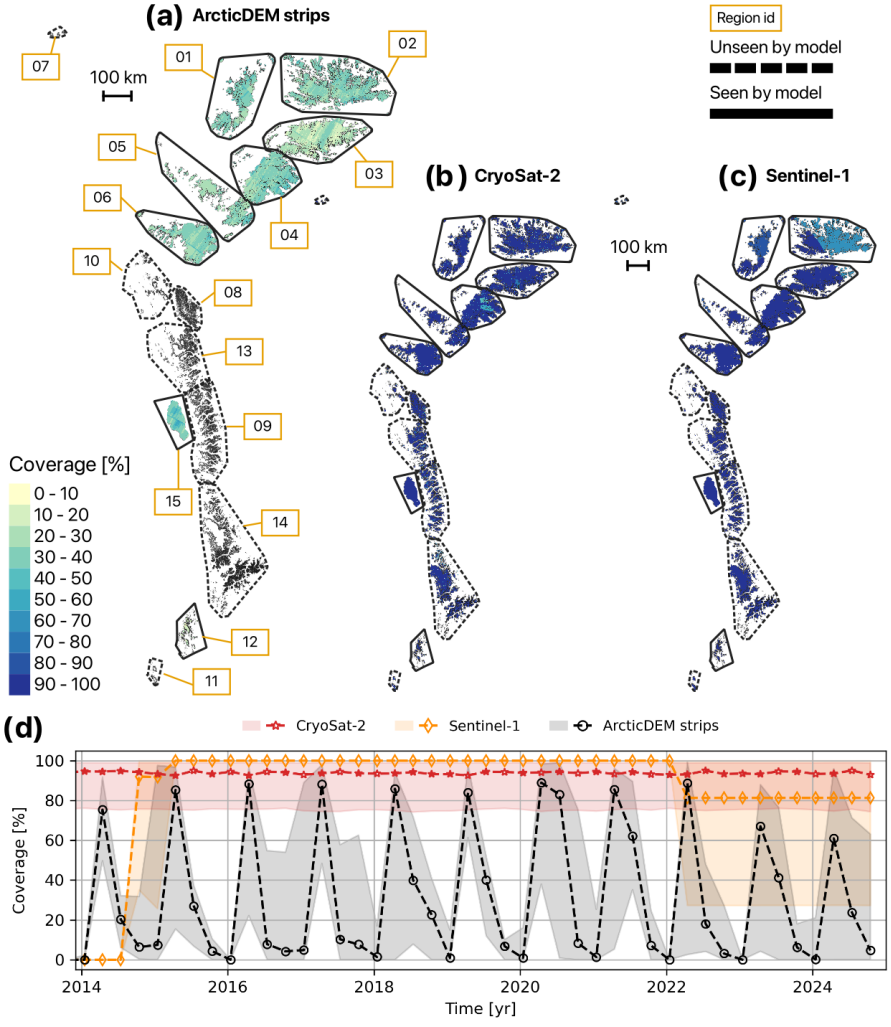


Figure 1. Spatial and temporal coverage of the input datasets across the Canadian Arctic. Panels (a)–(c) show the coverage percentage over the study period on a pixel-by-pixel basis for ArcticDEM strips, CryoSat-2, and Sentinel-1, respectively. Panel (a) only includes data in the regions used for model training (Regions 01–06, 12, and 15), whereas panels (b) and (c) include data of all study regions. Panel (d) summarizes the temporal coverage of the training regions for the three datasets, all aggregated into 3-month accumulations. Dashed lines show the mean coverage across the model regions and the shaded envelopes denote the minimum and maximum sub-regional coverage.

2 Data and pre-processing

In this section, we describe the datasets used to generate the U-DEM timeseries (100 m spatial resolution and 3-month temporal resolution), together with the preprocessing steps applied prior to model training. U-DEM combines information from three primary datasets: (i) CryoSat-2 swath elevations, which provide high temporal resolution elevation observations

https://doi.org/10.5194/egusphere-2026-5963
Preprint. Discussion started: 3 November 2026
© Author(s) 2026. CC BY 4.0 License.

(Sect. 2.2); (ii) Sentinel-1 backscatter imagery, which provides high-spatiotemporal-resolution information on glacier surface texture (Sect. 2.3); and (iii) ArcticDEM strips, which provide high-spatial-resolution elevation observations used as training targets (Sect. 2.4). In addition, the ArcticDEM mosaic serves as a reference DEM throughout the study (Sect. 2.1). Independent validation is performed using ICESat-2 elevation measurements (Sect. 2.5) and in-situ Global Navigation Satellite System (GNSS) observations (Sect. 2.6).

Throughout this study, time series are aggregated into four seasons: winter (December - February), spring (March - May), summer (June - August), and autumn (September - November). This means that data from e.g., December 2017 is part of the winter 2018 data. All datasets are processed in the WGS 84 / NSIDC Sea Ice Polar Stereographic North projection (EPSG:3413).

2.1 Reference elevation data

The 100 m ArcticDEM mosaic (Porter et al., 2023) is used as the reference elevation dataset throughout this study. It serves as the basis for outlier detection in the other datasets and provides elevation values for ice-free terrain outside the Randolph Glacier Inventory (RGI) version 7 glacier outlines (RGI Consortium, 2023). The mosaic is clipped for each sub-region (Fig. 1) and defines the spatial grid of each sub-region.

2.2 High temporal resolution elevation data: CryoSat-2

CryoSat-2 provides the high-temporal-resolution elevation observations used in U-DEM. CryoSat-2 carries a radar altimeter that measures surface elevations all year round, regardless of e.g., cloud cover and sunlight. Here, we use the swath-processed CryoSwath data product of the Canadian Arctic from Haacker and Wouters (2025), which yield a spatial resolution of 500 m and monthly temporal resolution, from the launch of the satellite in 2010 and until the end of 2024. Because the monthly coverage is spatially incomplete, observations are aggregated into seasonal (3-month) composites, which substantially reduces data gaps.

To create the desired seasonal timeseries of CryoSat-2, we first clean the data. The CryoSwath data product does not only include the height above the WGS84 ellipsoid, but also the error of the height estimate with respect to a reference DEM (ArcticDEM in the case of Arctic Canada). Therefore, to exclude outliers, we remove all points with an elevation error greater than 25 m. This chosen threshold is rather large to not exclude points of actual large elevation change, caused by for instance surging glaciers. This cleaned monthly dataset is used to generate both a "raw" dataset for model validation, as well as a gap-filled dataset used to train and run the model. For the raw dataset, seasonal medians are calculated throughout the entire time period and are interpolated onto the 100 m reference grid in a nearest neighbour manner, thus keeping the effective resolution at 500 m. The temporal and spatial coverage of CryoSat-2 for the entire region is shown in Fig. 1b and d.

As missing values can be difficult for convolutional neural networks to handle (Uhrig et al., 2017), we generate a second, gap-filled CryoSat-2 dataset for model training. Remaining gaps are filled using nearest-neighbour extrapolation up to a distance of 20 pixels. Although most gaps are only 1-3 pixels wide, the larger threshold ensures nearly complete spatial coverage. Because CryoSwath only provides elevations within the RGI v7 glacier mask, ice-free areas are assigned elevations from the

https://doi.org/10.5194/egusphere-2026-5963
Preprint. Discussion started: 3 November 2026
© Author(s) 2026. CC BY 4.0 License.

ArcticDEM mosaic after first coarsening the mosaic to the native 500 m CryoSwath resolution. The resulting DEMs are then interpolated onto the 100 m reference grid used by U-DEM.

2.3 High spatiotemporal resolution surface texture data: Sentinel-1

Sentinel-1 backscatter imagery is used to provide spatially detailed information on glacier surface texture and morphology, which may contain information related to local elevation variability. Unlike CryoSat-2, Sentinel-1 offers both high spatial and temporal resolution and is therefore used to provide the fine-scale spatial information required to downscale the coarser CryoSat-2 elevation observations.

We use Sentinel-1 Level-1 Ground Range Detected (GRD) imagery acquired in Extra Wide (EW) mode and horizontally polarized "HH". All ascending and descending acquisitions covering the study area are processed using Google Earth Engine (Gorelick et al., 2017). Preprocessing consists of border-noise removal followed by the calculation of seasonal mean backscatter composites. The seasonal composites are exported in their native 40 m resolution and in the WGS 84 / NSIDC Sea Ice Polar Stereographic North projection (EPSG:3413). Subsequently, all composites are resampled to the 100 m reference grid using weighted-average interpolation.

Unlike the CryoSat-2 elevations, the Sentinel-1 backscatter data are not gap-filled. The few gaps present in the record arise from incomplete spatial coverage during the early phase of the mission when only Sentinel-1A was operational, and after the failure of Sentinel-1B in December 2021. Because these gaps correspond to missing acquisition tracks rather than isolated missing pixels, they cannot be meaningfully reconstructed and are therefore retained in the dataset (Fig. 1c-d).

The resulting seasonal Sentinel-1 composites are used as an input channel to the U-Net, providing spatially continuous information on glacier surface characteristics that complements the coarser CryoSat-2 elevation observations.

2.4 High spatial resolution elevation data: ArcticDEM strips

ArcticDEM strips provide the high-spatial-resolution elevation information used to train U-DEM. Unlike CryoSat-2, ArcticDEM can resolve fine-scale glacier surface features and elevation gradients at meter-scale resolution, making it well suited as the target dataset that the U-Net aims to reproduce. However, because ArcticDEM strips rely on optical stereo imagery, their temporal coverage is irregular and dependent on cloud-free and sunlit conditions.

We use ArcticDEM strips version s2s041 (Porter et al., 2022), which are generated from stereo imagery acquired by the GeoEye-1 and WorldView satellites. Previous work has shown that strips generated from GeoEye-1 are often of lower quality (Zinck et al., 2023); therefore, only strips derived from the WorldView satellites are considered. To reduce storage requirements, the strips and their associated quality bitmasks are resampled to a 50 m grid using nearest-neighbour interpolation. Only pixels flagged as "good data" in the accompanying bitmask are retained. Furthermore, only strips covering regions used in training the model (Fig. 1) are downloaded.

Because ArcticDEM strips are not co-registered to a common elevation reference, individual strips may contain residual horizontal tilt and vertical bias relative to the true surface. A widely used approach to correct such errors is to fit a planar surface to the elevation residuals between a strip and a reference dataset, such as ground control points (Shean et al., 2019; Lilien et al.,

https://doi.org/10.5194/egusphere-2026-5963
Preprint. Discussion started: 3 November 2026
© Author(s) 2026. CC BY 4.0 License.

2024) or satellite altimetry observations (Zinck et al., 2023). Following this approach, we perform a two-step co-registration procedure using a reference DEM composed of the ArcticDEM mosaic over ice-free terrain and seasonal CryoSat-2 elevations over glacierized terrain. First, a planar surface is fitted to the residuals between each strip and the reference DEM, correcting large-scale tilt and vertical bias. A second co-registration is then performed using only residuals smaller than 15 m, thereby reducing the influence of outliers. Following co-registration, pixels differing by more than 25 m from the reference DEM are flagged as outliers and removed. No additional horizontal co-registration is performed, as previously reported horizontal geolocation offsets of approximately 3–5 m (Noh and Howat, 2015; Dai and Howat, 2017) are small relative to the 100 m resolution used in this study.

Despite the bitmask filtering and co-registration procedure, some contaminated strips and pixels may remain. Such contamination can arise from fog, low clouds, or other artefacts that are not identified by the quality bitmask. Because the ArcticDEM strips serve as training targets, these artefacts may cause the model to learn incorrect elevation patterns. To mitigate this issue, all strips are manually inspected and assigned a quality score: 1 (Excellent), 2 (Good), 3 (Poor), or 4 (Useless). Strips classified as useless are discarded. The remaining strips are used to generate a seasonal dataset by calculating a weighted average of all strips within a given season using weights of 1.0, 0.5, and 0.25 for Excellent, Good, and Poor strips, respectively. To increase the amount of training data available to the U-Net, small gaps in the dataset are filled. Compared to CryoSat-2, a more conservative gap-filling strategy is adopted because the ArcticDEM strips serve as the prediction target. Gaps are therefore only filled within a distance of five pixels using bilinear interpolation. The spatial and temporal coverage of the resulting dataset is shown in Fig. 1a,d. The dataset provides the high-spatial-resolution elevation information that the model seeks to reconstruct from CryoSat-2 and Sentinel-1 observations.

2.5 Independent satellite validation data

To independently evaluate the U-DEM elevation time series, we use ICESat-2 elevation measurements acquired from its launch in 2018 onward. ICESat-2 carries a laser altimeter that provides highly accurate surface elevation measurements over glacierized terrain and is therefore well suited for validating the reconstructed DEMs. We use the ATL06 Land Ice Height Version 7 product (Smith et al., 2025). Only observations flagged as good quality (`quality_summary = 0`) and with an estimated height error below 0.5 m are retained.

The ICESat-2 point observations are aggregated onto the 100 m spatial and seasonal (3-month) reference grid used throughout this study. For each grid cell and season, the median elevation of all ICESat-2 observations is calculated. Grid cells differing by more than 100 m from the ArcticDEM mosaic are considered outliers and removed. The resulting gridded ICESat-2 dataset serves as an independent satellite-based validation dataset for assessing the accuracy of the U-DEM elevation estimates.

2.6 Independent in-situ validation data

As an additional and particularly stringent validation, we compare the U-DEM elevations against kinematic GNSS measurements collected on White Glacier, Axel Heiberg Island, Nunavut (region 01, Fig. 1). White Glacier provides a challenging test case because its narrow geometry means that, over much of its length, the glacier is only 500-1000 m wide, corresponding

https://doi.org/10.5194/egusphere-2026-5963
Preprint. Discussion started: 3 November 2026
© Author(s) 2026. CC BY 4.0 License.

to one to two native CryoSat-2 pixels. Consequently, successful reconstruction of its elevation variability would demonstrate U-DEM's ability to recover spatial detail beyond the native resolution of the input altimetry data.

The validation dataset consists of six kinematic GNSS surveys conducted during the spring field seasons of 2015, 2017-2019, and 2023-2024. All surveys include measurements along the approximate glacier centerline, while several surveys also contain observations from tributary basins. Prior to analysis, the GNSS measurements are reprojected to the WGS 84 / NSIDC Sea Ice Polar Stereographic North projection (EPSG:3413). The resulting elevations provide an independent in-situ assessment of the accuracy of U-DEM and its ability to reproduce fine-scale elevation variations across narrow glacier geometries.

3 Methods

This section first describes the methodology behind U-DEM (Sect. 3.1), from data preparation (Sect. 3.1.1) and the U-Net architecture (Sect. 3.1.2) to the post-processing of the model output (Sect. 3.1.3). We then describe the validation of U-DEM against ICESat-2 and in-situ measurements (Sect. 3.2), before presenting the methodology used for the U-DEM application examples (Sect. 3.3).

We have divided the Canadian Arctic into 15 sub-regions (Fig. 1), which we use to both make data handling easier, but also to do sub-regional validation. Furthermore, we only use a subset of the regions (01-06, 12, and 15) in the training of the model, but apply the final U-DEM model to all regions. Validation with respect to ICESat-2 is done for all regions, which also allow us to inspect how well the model performs in regions that are entirely unseen by the model.

3.1 U-DEM

3.1.1 Data preparation

To prepare the input data for the U-Net, the gap-filled elevation and texture datasets are normalized, tiled, and split up as follows.

The elevation data, including both ArcticDEM strips and CryoSat-2, are first converted to elevation residuals by subtracting the ArcticDEM mosaic. This transformation allows the model to learn elevation anomalies rather than absolute elevations, thereby focusing the learning process on temporal and local deviations from the mean ice-surface geometry. The elevation residuals are subsequently normalized on a per-region basis according to

$$r_{norm} = \frac{r - \mu_{r_{cs}}}{\sigma_{r_{cs}}}, \tag{1}$$

where r_{norm} is the normalized elevation residual, r is the elevation residual, and $\mu_{r_{cs}}$ and $\sigma_{r_{cs}}$ are the mean and standard deviation of all CryoSat-2 residual observations within the spatial and temporal domain of a given sub-region. These statistics are computed across the entire sub-region rather than on a pixel-by-pixel basis. Consequently, both the CryoSat-2 and ArcticDEM residuals are normalized using the same regional CryoSat-2 mean and standard deviation. Sentinel-1 backscatter data are normalized in an analogous manner, but on a pixel-by-pixel basis using their own pixel mean and standard deviation.

https://doi.org/10.5194/egusphere-2026-5963
Preprint. Discussion started: 3 November 2026
© Author(s) 2026. CC BY 4.0 License.

To be used as input to the U-Net, the data must first be divided into smaller tiles. Using the entire study region as a single input would require complete spatial coverage from all input datasets, whereas tiling allows the model to be trained on smaller regions where data are available. In addition, tiling increases the number of training samples available to the model. Choosing an appropriate tile size involves a trade-off as tiles must be large enough to capture relevant spatial features while remaining small enough to ensure computational feasibility. Furthermore, predictions near tile boundaries can be affected by edge artifacts arising from the limited spatial context available at the tile borders. Through trial and error, we found an optimal tile size of 128 $\times$ 128 pixels, corresponding to 12.8 $\times$ 12.8 km. To further reduce boundary effects, we require all tiles located along glacier margins to contain at least a 16-pixel buffer between the tile edge and the nearest ice-covered pixel, as defined by the RGI outlines. Finally, adjacent tiles are constructed with an overlap of 72 pixels to ensure continuous spatial coverage and minimize seam artifacts when reconstructing the full-domain. Figure A1 in App. A illustrates an example of how the tiles overlap each other.

The resulting tiles are then divided into training and internal validation datasets, with 90% of the tiles used for model training and the remaining 10% used for internal validation, using a random train-test splitting. The internal validation dataset is also used for hyperparameter optimization. For this purpose, it is further divided into 80% training and 20% validation subsets. Independent evaluation of the trained model is subsequently performed using ICESat-2 observations (Sect. 3.2), which are not used at any stage of model training or hyperparameter optimization.

3.1.2 U-Net

U-DEM is based on an Attention U-Net architecture (Ronneberger et al., 2015; Oktay et al., 2018). As illustrated in Fig. 2, the network takes two input channels, Sentinel-1 backscatter and CryoSat-2 elevation residuals, and predicts a single channel of ArcticDEM strip elevation residuals. Both input and output tiles have dimensions of 128 $\times$ 128 pixels, corresponding to 12.8 $\times$ 12.8 km at 100 m spatial resolution.

The network consists of four encoder levels, a bottleneck, and four decoder levels connected by attention-gated skip connections. Each encoder level contains two 3 $\times$ 3 convolutions with one-pixel zero padding and Leaky Rectified Linear Unit (LeakyReLU) activation, followed by 2 $\times$ 2 max pooling. Batch normalization and spatial dropout are optionally applied depending on the hyperparameter configuration. The number of feature channels doubles at each encoder level, while the spatial dimensions are halved. The bottleneck is followed by a symmetric decoder in which the feature maps are bilinearly upsampled and combined with the corresponding encoder features through attention-gated skip connections (Oktay et al., 2018). A final 1 $\times$ 1 convolution maps the decoder features to the predicted elevation residuals. With the optimal hyperparameters described in Tab. 1, the final network contains 2,205,749 trainable parameters. The theoretical receptive field along the encoder path reaches 140 $\times$ 140 input pixels after the second convolution in the bottleneck and therefore encompasses the full 128 $\times$ 128 pixel input tile.

For both hyperparameter optimization and final model training, the network parameters are updated using the Adam optimizer (Kingma and Ba, 2017). The optimizer minimizes a loss function combining the mean absolute error (MAE) and mean

https://doi.org/10.5194/egusphere-2026-5963
Preprint. Discussion started: 3 November 2026
© Author(s) 2026. CC BY 4.0 License.

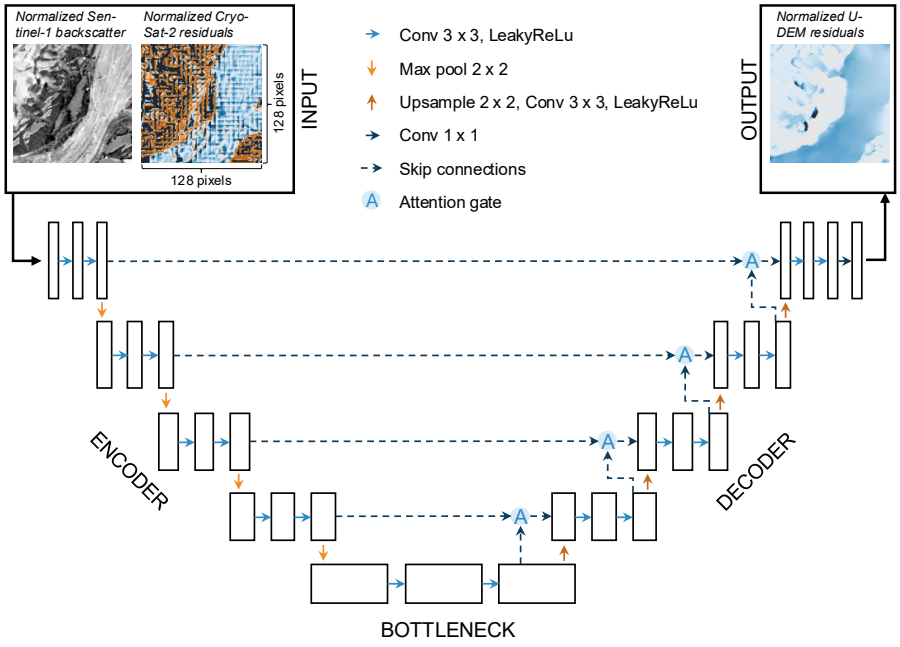


Figure 2. Architecture of the Attention U-Net used to generate U-DEM. The network takes 128 × 128 pixel tiles of normalized CryoSat-2 elevation residuals and normalized Sentinel-1 backscatter as input and predicts normalized elevation residuals at 100 m spatial resolution. Colored arrows indicate the different network operations shown in the legend.

squared error (MSE) with equal weights,

$$\mathcal{L} = \frac{1}{2N}\sum_{i=1}^{N}|y_i - \hat{y}_i| + \frac{1}{2N}\sum_{i=1}^{N}(y_i - \hat{y}_i)^2, \tag{2}$$

where y_i and $\hat{y}_i$ denote the target ArcticDEM strip and predicted normalized elevation residuals, respectively, and N is the number of elements included in the loss calculation. Combining the two terms balances the robustness of the MAE to local outliers with the stronger penalization of large prediction errors provided by the MSE.

Network hyperparameters are optimized using Optuna (Tree-structured Parzen Estimator, Akiba et al., 2019), which employs Bayesian optimization to explore the hyperparameter space. The optimization is performed exclusively using the internal validation dataset described in Sect. 3.1, and the explored search space and resulting optimal values are listed in Table 1. The optimized parameters control regularization (batch normalization and dropout), optimization (learning rate, batch size, and number of epochs), and network capacity (number of base filters). To satisfy GPU memory constraints, only combinations for which *batch size* × *base filters* ≤ 512 are evaluated.

Following hyperparameter optimization, the model is trained on the complete training dataset using the optimal hyperparameter configuration, with the internal validation dataset used to evaluate model performance during training. The best model parameters can be found in Tab. 1. The trained network is subsequently applied to all available CryoSat-2 and Sentinel-1 observations to generate the seasonal U-DEM time series for all 15 study regions.

https://doi.org/10.5194/egusphere-2026-5963
Preprint. Discussion started: 3 November 2026
© Author(s) 2026. CC BY 4.0 License.

Table 1. Hyperparameter search space explored by Optuna and the resulting optimal values. Curly braces, {}, denote categorical search spaces, square brackets, [ ], denote continuous search intervals sampled logarithmically and regular brackets, ( ), denote continuous search intervals sampled linearly.

Parameter	Search space	Optimal value
Batch normalization	$\{\mathrm{True}, \mathrm{False}\}$	True
Dropout	$\{\mathrm{True}, \mathrm{False}\}$	False
Dropout rate[†]	$(0.05, 0.6)$	–
Learning rate	$[10^{-4}, 5 \cdot 10^{-2}]$	$\approx 8.98 \cdot 10^{-4}$
Batch size[*]	$\{4, 8, 16, 32\}$	16
Base filters[*]	$\{8, 16, 32, 64\}$	16
Epochs	$(50, 200)$	186

[†]Only when *Dropout* $= \mathrm{True}$.
[*]Only hyperparameter combinations satisfying *batch size* $\cdot$ *base filters* ≤ 512 were evaluated to satisfy GPU memory constraints.

3.1.3 Post-processing

The U-Net predicts normalized elevation residuals for individual 128 × 128 pixel tiles. To obtain absolute glacier elevations, the predicted residuals are first denormalized using the regional CryoSat-2 mean and standard deviation before adding the ArcticDEM mosaic.

The resulting elevation tiles are subsequently mosaicked into seasonal DEMs for each study region. Because predictions near tile boundaries are more susceptible to edge artefacts arising from the limited spatial context available at the tile borders, overlapping predictions are combined using a distance-weighted average. This follows the general approach of Mohajerani et al. (2021), who similarly reduce the influence of tile-edge predictions during mosaicking, but use Gaussian rather than distance-based weighting. For each tile, the weight assigned to a pixel increases linearly with its distance from the nearest tile edge, from a minimum of 0.1 at the tile boundary to a maximum of 1 at the tile centre. Where multiple tiles overlap, the predicted elevations are averaged according to these weights (see example in Fig. A1). This gives greater influence to predictions near tile centres, where more surrounding spatial context is available to the network, while retaining information from the complete 128 × 128 pixel prediction tiles.

3.2 DEM validation

The performance of U-DEM is evaluated using two independent validation datasets: (i) ICESat-2 elevations and (ii) kinematic GNSS measurements from White Glacier. For reference, the same validation procedures are also applied to the raw CryoSat-2 elevations, allowing the performance of U-DEM to be assessed relative to its primary elevation input.

https://doi.org/10.5194/egusphere-2026-5963
Preprint. Discussion started: 3 November 2026
© Author(s) 2026. CC BY 4.0 License.

Validation against ICESat-2 is performed on both individual regions and the combined dataset using the root-mean-square error (RMSE), bias, and coefficient of determination (R^2). To further assess the temporal robustness of U-DEM, the ICESat-2 validation is also carried out separately for each season. This analysis serves two purposes. First, it evaluates whether the model has learned to reduce the seasonal penetration-depth bias present in the CryoSat-2 observations. Second, it assesses whether the uneven seasonal distribution of the ArcticDEM training data, which is dominated by spring and summer acquisitions, influences model performance. In addition, elevation residuals with respect to ICESat-2 are analysed as a function of surface slope and surface elevation to investigate how model performance varies with terrain characteristics.

Finally, U-DEM is compared with the kinematic GNSS surveys on White Glacier. For comparison, CryoSat-2 elevations and all available ArcticDEM strips are evaluated in the same manner. Prior to the comparison, all elevation datasets are linearly interpolated onto the GNSS survey tracks, after which elevation residuals are calculated with respect to the GNSS measurements.

3.3 Application examples

To demonstrate the capabilities of U-DEM for investigating glacier dynamics at different spatial scales, we consider two application examples. First, we examine elevation changes associated with three known surge-type glaciers: Iceberg Glacier (Lauzon et al., 2023), Mittie Glacier (Copland et al., 2024), and Chapman Glacier (Van Wychen et al., 2025). For each glacier, U-DEM elevation profiles are extracted along RGI v7 glacier centrelines to investigate the spatial and temporal evolution of elevation changes throughout the surge cycle.

Second, we investigate elevation changes associated with mapped active subglacial lakes in the Canadian Arctic (Zheng et al., 2026). For each lake, the mean surface elevation within the lake extent identified by Zheng et al. (2026) is calculated for U-DEM, CryoSat-2, and the available ArcticDEM strips. The resulting elevation time series are compared to assess how well U-DEM captures the localized elevation changes associated with subglacial lake drainage and refilling relative to the two other elevation datasets.

4 Results

4.1 Validation

The validation of U-DEM against independent ICESat-2 elevations (Fig. 3a) yields an RMSE of 10.01 m and a bias of -0.27 m. This represents a substantial improvement over the underlying CryoSat-2 elevations (Fig. 3b), which have an RMSE of 28.39 m, corresponding to a roughly 65% reduction in RMSE. Both products exhibit only small mean biases with respect to ICESat-2. The remaining RMSE should be interpreted in light of differences in spatial and temporal sampling between the datasets, as U-DEM represents elevations over 100 $\times$ 100 m grid cells and 3-month periods, whereas ICESat-2 provides measurements along narrow ground tracks acquired at discrete times. The implications of these sampling differences for the validation are discussed further in Sect. 5.

https://doi.org/10.5194/egusphere-2026-5963
Preprint. Discussion started: 3 November 2026
© Author(s) 2026. CC BY 4.0 License.

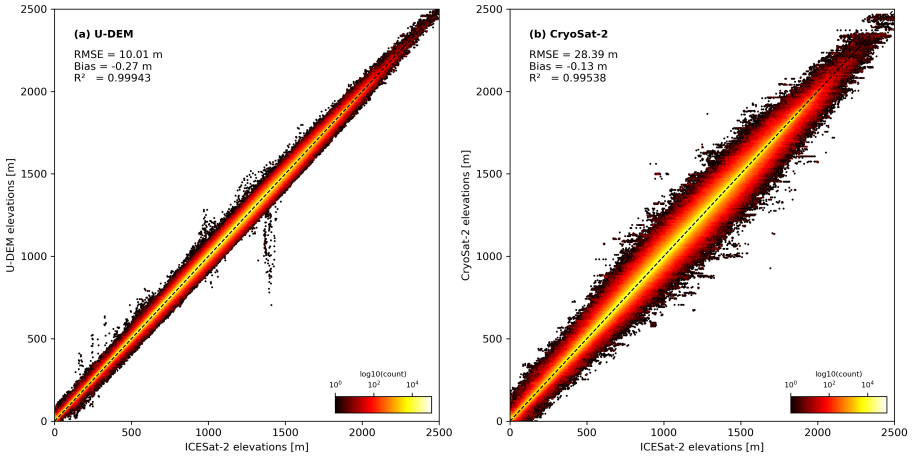


Figure 3. The independent ICESat-2 elevations versus **(a)** U-DEM and **(b)** CryoSat-2 for all regions combined.

Table 2. Seasonal validation statistics compared to ICESat-2. A positive bias correspond to an overestimation of elevation compared to ICESat-2.

Product	Season	RMSE [m]	Bias [m]	R^2
U-DEM	Winter	10.09	-0.20	0.9994
	Spring	10.13	-0.36	0.9994
	Summer	9.70	-0.46	0.9995
	Autumn	9.99	-0.13	0.9994
CryoSat-2	Winter	28.92	0.10	0.9952
	Spring	28.51	-0.11	0.9953
	Summer	27.35	-0.49	0.9957
	Autumn	28.28	-0.17	0.9954

Given the uneven seasonal distribution of ArcticDEM strips (Fig. 1) and the potential for seasonally varying radar penetration to affect CryoSat-2 elevations, we additionally evaluate U-DEM against ICESat-2 separately for each season (Tab. 2). This allows us to assess both whether the seasonal distribution of the training data affects model performance and whether potential seasonal biases in the CryoSat-2 input are propagated into U-DEM. U-DEM shows little seasonal variation in RMSE, with values remaining close to the overall RMSE of 10.01 m throughout the year. Bias also remains close to zero, ranging from -0.13 to -0.46 m, with no clear seasonal pattern. CryoSat-2 similarly shows little seasonal variation in RMSE or bias. The ICESat-2 validation therefore provides no evidence of substantial seasonal degradation in U-DEM performance or of a seasonally varying elevation bias that could indicate the propagation of CryoSat-2 penetration effects into U-DEM.

https://doi.org/10.5194/egusphere-2026-5963
Preprint. Discussion started: 3 November 2026
© Author(s) 2026. CC BY 4.0 License.

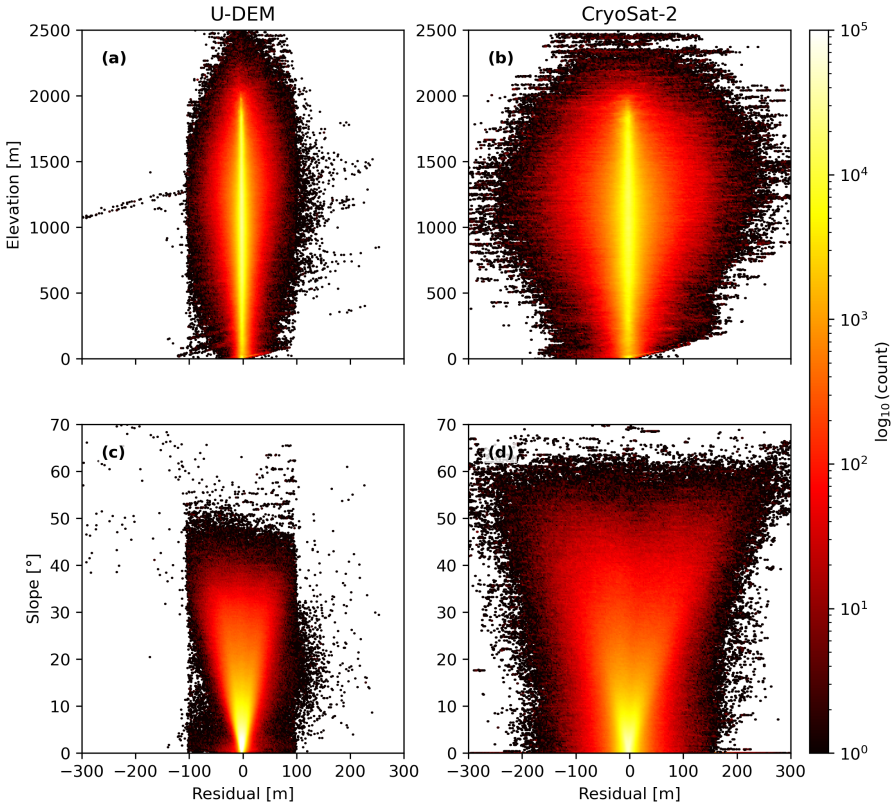


Figure 4. Elevation residual with respect to ICESat-2 as a function of elevation for **(a)** U-DEM and **(b)** CryoSat-2, and as a function of surface slope for **(c)** U-DEM and **(d)** CryoSat-2. Positive residual correspond to elevation overestimation compared to ICESat-2. The relatively sharp vertical lines in (a) and (c) are a result of filtering out ICESat-2 elevations deviating more than 100 m from the ArcticDEM mosaic.

To investigate whether the remaining differences with respect to ICESat-2 are associated with terrain characteristics, we examine U-DEM and CryoSat-2 residuals as a function of surface elevation and slope (Fig. 4). Residuals show limited systematic dependence on elevation, whereas their magnitude increases with surface slope for both products. CryoSat-2 generally shows larger residuals than U-DEM across the full range of slopes, with the largest differences occurring in the steepest terrain. This behaviour is consistent with the coarser spatial resolution of CryoSat-2 and its preferential sampling of surface locations closest to the satellite, which can lead to larger elevation differences in steep and topographically complex terrain (Haacker et al., 2023).

We further evaluate agreement with ICESat-2 separately for each of the 15 sub-regions to assess the spatial consistency of U-DEM and its generalization beyond the regions represented during training (App. B; Figs. B1 and B2). U-DEM outperforms CryoSat-2 in all sub-regions, reducing regional RMSE by 61-75%. U-DEM RMSE ranges from 2.30 m in region 15 to 13.21 m in region 08, compared with 9.35-43.68 m for CryoSat-2. Similar improvements occur in regions 07-11 and 13-14, which were not represented during model training, demonstrating that the improvement is not restricted to the training regions.

https://doi.org/10.5194/egusphere-2026-5963
Preprint. Discussion started: 3 November 2026
© Author(s) 2026. CC BY 4.0 License.

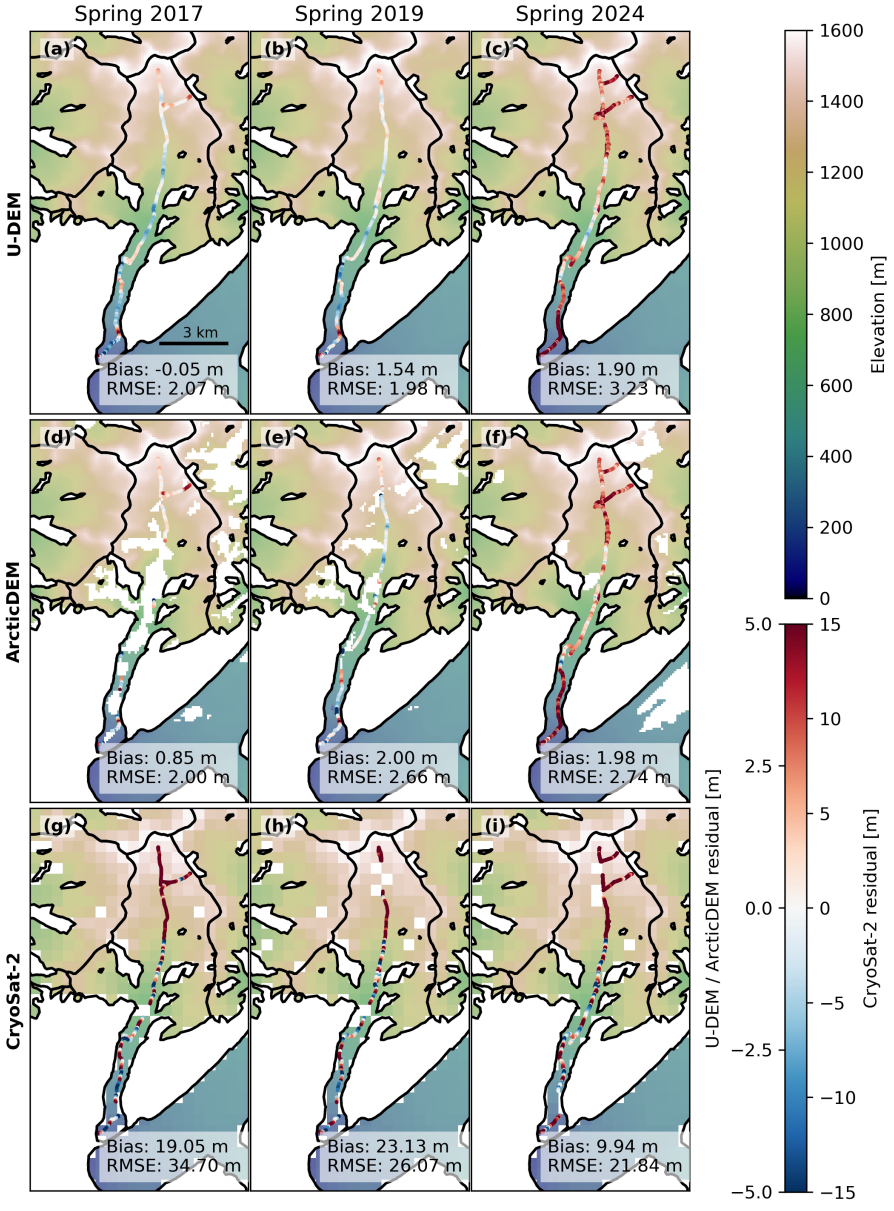


Figure 5. Comparison of U-DEM **(a-c)**, ArcticDEM **(d-f)** and CryoSat-2 **(g-i)** with respect to the kinematic GNSS surveys of White Glacier. Each column represent different campaign periods. Be aware that the residual colorbar for U-DEM and ArcticDEM ranges from -5 m to 5 m, whereas it ranges from -15 m to 15 m for CryoSat-2. Positive bias/residual indicate an overestimation of the surface elevation compared to the GNSS measurements. Fig. B3 shows a comparison of all years available.

As an additional independent validation, we compare U-DEM with six kinematic GNSS surveys of White Glacier (Fig. 5a-c and Fig. B3a-f). Across the six surveys, U-DEM biases range from -0.05 m in spring 2017 to 2.02 m in spring 2023,

https://doi.org/10.5194/egusphere-2026-5963
Preprint. Discussion started: 3 November 2026
© Author(s) 2026. CC BY 4.0 License.

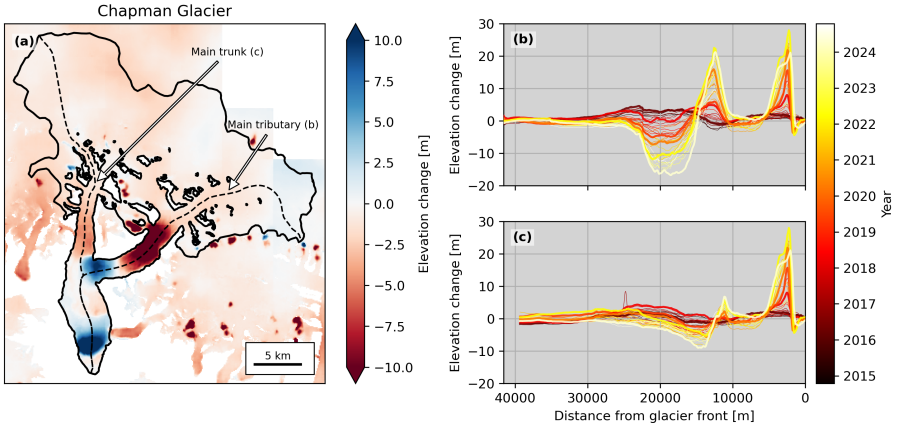


Figure 6. Multiphase surge of Chapman Glacier, Ellesmere Island. **(a)** U-DEM elevation change between fall 2014 and fall 2024 of Chapman Glacier, marked by the black outline from RGI v7 (RGI Consortium, 2023). The dashed lines are RGI v7 centrelines, of the main tributary plotted in b) and the main trunk plotted in c). **(b)** U-DEM elevation change of the main tributary marked in a) with respect to fall 2014. **(c)** U-DEM elevation change of the main trunk marked in a) with respect to fall 2014. The following springs are marked by thicker lines in b) and c): 2016, 2018, 2019, 2020, 2022, 2024.

with RMSE values of 1.70-3.35 m. These errors are comparable to those of ArcticDEM over the same profiles (Fig. 5d-f and Fig. B3g-l), with biases of -0.55-2.00 m and RMSE values of 1.43-2.74 m. The comparable performance indicates that U-DEM recovers much of the spatial elevation information provided by the high-resolution ArcticDEM strips.

In contrast, CryoSat-2 shows substantially larger differences from the GNSS measurements (Fig. 5g-i and Fig. B3m-r), with RMSE values of 21.84-34.70 m and predominantly positive biases of 2.55-23.13 m. The largest overestimations occur in the upper part of White Glacier, where the GNSS track follows a relatively low-elevation part of the glacier bordered by higher terrain. CryoSat-2 elevations are consequently biased towards the surrounding higher terrain, despite the use of swath processing. U-DEM substantially reduces these differences and more closely reproduces the GNSS elevations along the glacier.

4.2 Applications

To demonstrate the ability of U-DEM to resolve glacier dynamics at high spatial and temporal resolution, we examine the ongoing multiphase surge of Chapman Glacier, Ellesmere Island (region 02, Fig. 1). Van Wychen et al. (2025) identified an initial surge of the main trunk from 2001 to 2012, followed by acceleration of the main tributary from around 2012 that propagated down-glacier and eventually affected the lower main trunk. However, the available elevation observations could not resolve the position and migration of the dynamic balance line separating surge-related surface lowering and thickening.

U-DEM elevation changes of Chapman Glacier between fall 2014 and fall 2024 show pronounced spatial patterns, in three-months interval, of ice redistribution associated with the ongoing second surge phase (Fig. 6a). The main tributary shows substantial surface lowering upstream and thickening downstream, consistent with down-glacier ice transfer during the surge.

https://doi.org/10.5194/egusphere-2026-5963
Preprint. Discussion started: 3 November 2026
© Author(s) 2026. CC BY 4.0 License.

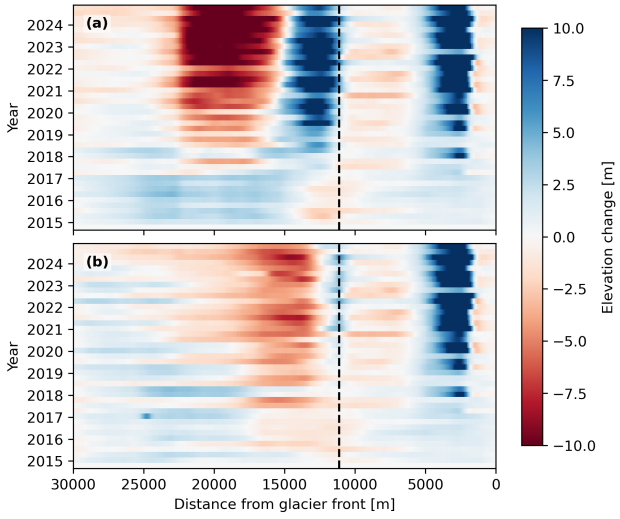


Figure 7. Hovmöller diagram showing Chapman Glacier elevation change from U-DEM of each time step with respect to fall 2014 of **(a)** the main trunk and **(b)** the main tributary marked in Fig. 6a. The dashed vertical line indicates the point at which the two centrelines merge.

The elevation profiles show the development of these patterns through time (Fig. 6b-c), with the boundary between lowering and thickening marking a dynamic balance line that progressively migrates down-glacier.

This migration is particularly apparent in the Hovmöller diagrams (Fig. 7). Along the main tributary, surface lowering progressively expands down-glacier from approximately 2018 onwards, accompanied by migration of the dynamic balance line and downstream thickening ahead of it (Fig. 7a). By 2020, positive elevation changes extend across the confluence, indicating that ice redistribution associated with the tributary surge has reached the central main trunk. Changes along the main trunk are more subtle, although substantial thickening develops in the lower section shared by the two profiles (Fig. 7b). The 3-monthly time series thus resolves the progressive migration of the dynamic balance line that could not be determined from the temporally incomplete elevation observations available in previous studies.

As additional examples, the elevation evolutions of Iceberg and Mittie glaciers are shown in App. C (Figs. C1 and C2, respectively). Both glaciers are currently in their quiescent phases, providing examples of the elevation-change patterns captured by U-DEM outside the active surge phase.

We additionally use the active subglacial lakes identified in the Canadian Arctic by Zheng et al. (2026) to test the ability of U-DEM to resolve smaller-scale and potentially short-lived elevation changes. Drainage and refilling produce localized surface lowering and uplift, respectively, providing a demanding test of the spatial resolution of U-DEM. From the more than 30 identified lakes, we select four examples representing the range of performance across the dataset (Fig. 8).

For the first two lakes (Fig. 8a-b), U-DEM reproduces much of the temporal elevation variability observed by ArcticDEM, whereas CryoSat-2 shows little corresponding variability. For the third lake (Fig. 8c), U-DEM captures part, but not the full magnitude, of the variability observed by ArcticDEM, while still improving upon CryoSat-2. In the fourth example (Fig. 8d),

https://doi.org/10.5194/egusphere-2026-5963
Preprint. Discussion started: 3 November 2026
© Author(s) 2026. CC BY 4.0 License.

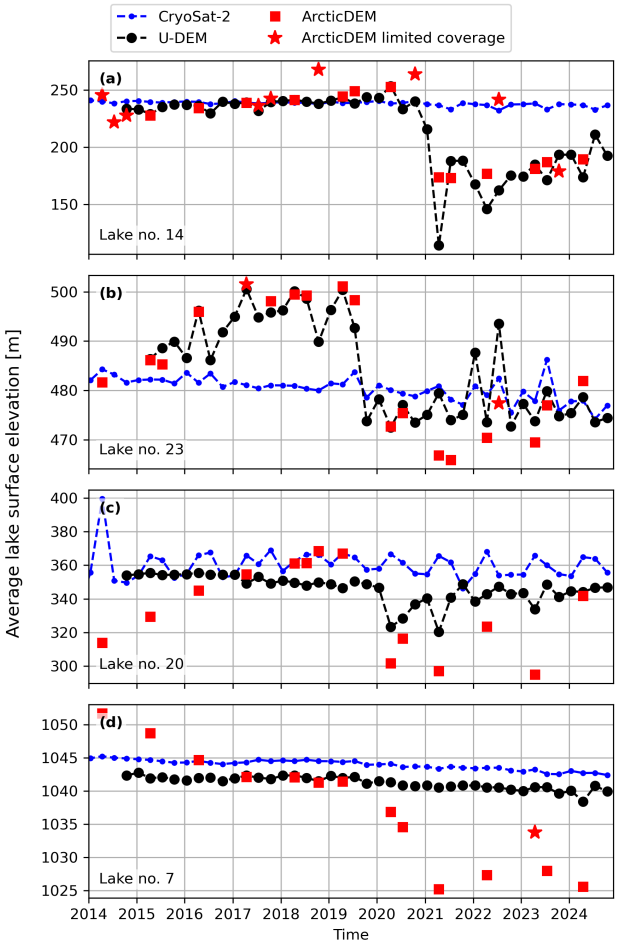


Figure 8. Average lake surface elevation of four subglacial lakes as defined by Zheng et al. (2026), comparing the lake elevation of CryoSat-2, ArcticDEM strips (when available), and U-DEM. Instances where the ArcticDEM strips cover less than 70% of the lake are marked by stars. The lake numbers correspond to the same lake numbers used in Zheng et al. (2026).

neither U-DEM nor CryoSat-2 captures the changes apparent in ArcticDEM. These examples demonstrate that U-DEM can recover localized elevation variability not resolved by CryoSat-2, but that this capability is not consistent across all lakes. Several mapped lakes have areas of only a few square kilometres, approaching scales poorly resolved by the CryoSat-2 observations and for which U-DEM increasingly relies on the spatial information provided by Sentinel-1.

5 Discussion

U-DEM provides a new machine-learned elevation time series for glaciers and ice caps in the Canadian Arctic at 100 m spatial and 3-month temporal resolution. U-DEM substantially improves upon the spatially coarse CryoSat-2 elevations and performs

https://doi.org/10.5194/egusphere-2026-5963
Preprint. Discussion started: 3 November 2026
© Author(s) 2026. CC BY 4.0 License.

consistently across the Canadian Arctic, including in regions not represented during model training (Figs. 3, B1, and B2). This improvement is further supported by the independent White Glacier GNSS validation, where U-DEM yields RMSE values of 1.70-3.35 m, comparable to those obtained for the ArcticDEM strips and substantially lower than for CryoSat-2 (Fig. 5). The higher RMSE of 10.01 m obtained against ICESat-2 should therefore not be interpreted solely as U-DEM elevation uncertainty, but also in the context of how the ICESat-2 observations were aggregated for validation. ICESat-2 samples elevations along narrow ground tracks, and the observations assigned to a 100 × 100 m pixel may cover only a small part of that pixel. The resulting ICESat-2 elevation may therefore not be representative of the elevation across the entire area represented by the corresponding U-DEM pixel, particularly in areas with strong local topographic gradients. This interpretation is consistent with the increasing magnitude of the ICESat-2 residuals with surface slope (Fig. 4). Together, the validation results indicate that U-DEM recovers much of the fine-scale spatial elevation information absent from CryoSat-2.

U-DEM builds on a growing effort to overcome the trade-off between spatial and temporal resolution in satellite-derived glacier elevation products. A closely related example is PRODEM (Winstrup et al., 2024), which combines CryoSat-2 and ICESat-2 altimetry with ArcticDEM to produce annual summer DEMs at 500 m resolution for the marginal areas of the Greenland Ice Sheet. U-DEM advances this concept by increasing both the spatial and temporal resolution of the reconstructed elevation fields. Rather than relying on spatial interpolation of satellite altimetry, U-DEM uses machine learning to infer high-resolution elevation patterns from CryoSat-2 elevations and Sentinel-1 backscatter, with ArcticDEM strips providing high-resolution training targets. This enables elevations to be reconstructed at 100 m spatial and 3-month temporal resolution, compared with the 500 m annual summer DEMs provided by PRODEM, thereby resolving smaller-scale spatial features and their evolution within individual years. In addition, U-DEM does not use ICESat-2 as an input, allowing it to remain fully independent for validation. U-DEM therefore represents a further step towards simultaneously resolving the spatial detail and temporal evolution of glacier surface topography that cannot be captured by individual satellite elevation datasets.

The Chapman Glacier application demonstrates the value of combining high spatial and temporal resolution for studying rapidly evolving glacier dynamics. While Van Wychen et al. (2025) identified the propagation of the ongoing surge from the tributary towards the main trunk, the available observations did not allow the position and migration of the dynamic balance line to be resolved through time. The 3-monthly U-DEM series resolves its progressive down-glacier migration and the subsequent propagation of thickening into the main trunk, providing a more continuous view of ice redistribution during the surge (Fig. 6 and 7). More generally, analyses of surge evolution often require several elevation datasets with different spatial resolutions, acquisition frequencies, and sampling characteristics to constrain changes in glacier geometry through time. U-DEM provides a single, consistent elevation time series from which the spatial propagation and timing of such changes can be followed at seasonal resolution, thereby reducing the need to combine multiple elevation products. While complementary observations, particularly ice velocity, remain important for interpreting glacier dynamics, U-DEM can provide much of the spatial and temporal elevation information required to characterize rapidly evolving glacier geometry.

The subglacial-lake analysis (Fig. 8), in contrast, highlights both the potential and spatial limitations of U-DEM. Zheng et al. (2026) used ArcticDEM strips to identify and characterize active subglacial lakes across the Canadian Arctic, but noted that their irregular temporal coverage limits the ability to constrain the timing of short-lived drainage events. The 3-monthly

https://doi.org/10.5194/egusphere-2026-5963
Preprint. Discussion started: 3 November 2026
© Author(s) 2026. CC BY 4.0 License.

U-DEM series could help bridge these temporal gaps and, for several lakes, resolves localized elevation changes that are absent from CryoSat-2. However, U-DEM only partly or not at all reproduces the changes observed by ArcticDEM for some lakes. Because these localized features are poorly resolved by CryoSat-2, U-DEM's spatial reconstruction likely relies strongly on spatial gradients in Sentinel-1 backscatter from which the network can infer fine-scale surface structure. However, Sentinel-1 backscatter is strongly affected by snow wetness and surface melt, with liquid water increasing radar attenuation and substantially altering the spatial backscatter signal (e.g., Carletti et al., 2025; Brangers et al., 2024). During such conditions, backscatter contrasts associated with local surface geometry may therefore become less distinct or be masked by variations related to surface conditions. This could weaken the spatial information available to U-DEM and explain why the model sometimes captures the occurrence of a subglacial-lake drainage event but underestimates its full elevation change. U-DEM therefore offers improved temporal sampling compared with ArcticDEM for monitoring subglacial-lake evolution, but should be used cautiously for features approaching its effective spatial resolution and preferably corroborated with independent elevation observations.

Beyond the examples presented here, the high spatiotemporal resolution of U-DEM enables a range of other applications. The temporally resolved surface geometry could, for example, improve inverse modelling of glacier bed topography, particularly for highly dynamic and surge-type glaciers where substantial ice redistribution means that a static DEM may not adequately represent the glacier geometry at a given time. Similarly, the 3-monthly elevation series provides a spatially continuous constraint for transient glacier modelling, allowing simulations to be evaluated against seasonal to interannual changes in glacier geometry rather than individual, temporally sparse DEM acquisitions.

Beyond these applications, the approach used to produce U-DEM could potentially be transferred to other glacierized regions. The required datasets already exist across much of the Arctic and Antarctic, with CryoSat-2 and Sentinel-1 providing temporally repeated observations and ArcticDEM strips or the Reference Elevation Model of Antarctica (REMA) strips providing high-resolution elevation data for model training. Direct application of the model trained here to substantially different glaciological environments should, however, be approached cautiously, as glacier geometry, surface conditions, and Sentinel-1 backscatter characteristics may differ considerably between the Canadian Arctic, the Greenland and Antarctic ice sheets, and ice shelves. Retraining the network using ArcticDEM or REMA strips from the target region would therefore likely be necessary. Furthermore, while the current U-DEM network is trained using CryoSat-2 and Sentinel-1 as inputs, the framework could be adapted to incorporate other existing or future satellite observations. For example, the upcoming Copernicus Polar Ice and Snow Topography Altimeter (CRISTAL, Kern et al., 2020) mission could complement or eventually replace CryoSat-2 as the radar-altimetry input, while additional datasets could be introduced as new input channels. For such efforts one can take departure in the pre-trained weights found here. The U-DEM framework therefore provides a flexible approach for combining complementary satellite observations and could evolve as new datasets become available.

6 Conclusions

We present U-DEM, a machine-learned glacier elevation time series for the Canadian Arctic at 100 m spatial and 3-month temporal resolution from 2014 to 2024. By combining CryoSat-2 elevations, Sentinel-1 backscatter, and ArcticDEM strips,

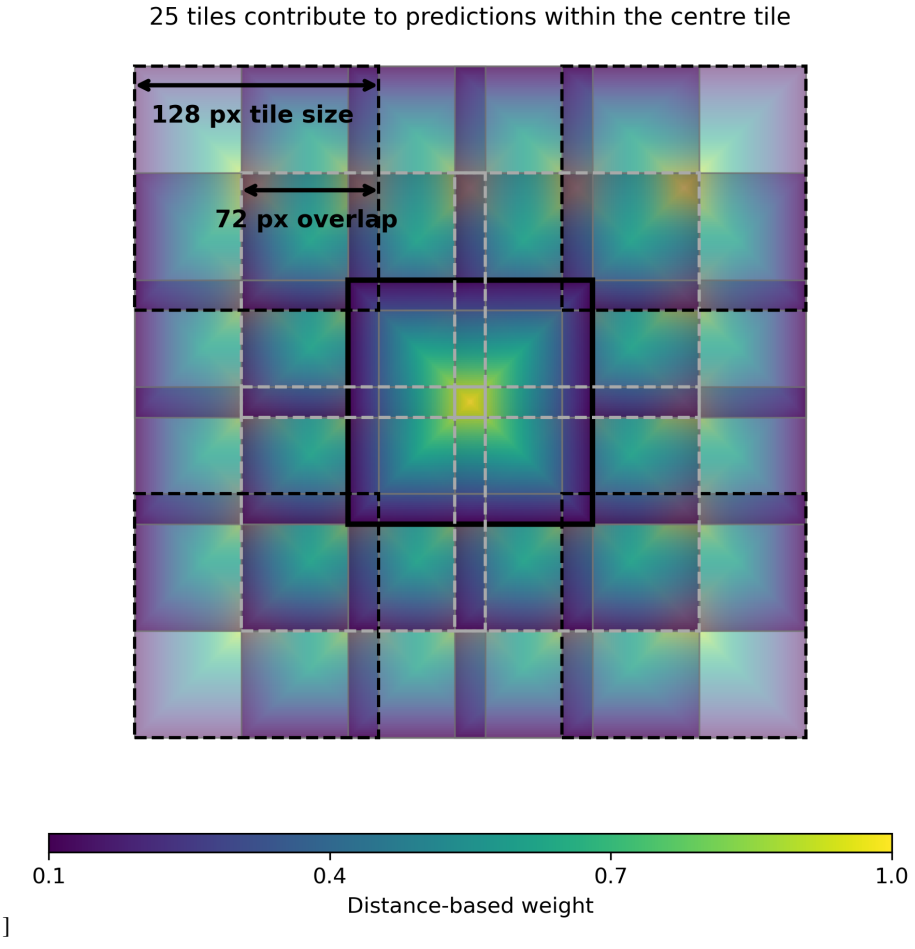
https://doi.org/10.5194/egusphere-2026-5963
Preprint. Discussion started: 3 November 2026
© Author(s) 2026. CC BY 4.0 License.

U-DEM bridges the trade-off between spatial and temporal resolution of existing elevation datasets. Validation against independent ICESat-2 observations shows a 65% reduction in RMSE relative to CryoSat-2, with improvements across all study regions, including those not represented during training. At White Glacier, U-DEM achieves RMSE values of 1.70-3.35 m, comparable to ArcticDEM despite the glacier being poorly resolved by CryoSat-2.

The resulting elevation time series resolves spatial and temporal patterns of glacier change that are difficult to capture with existing datasets individually, including the migration of the dynamic balance line during the ongoing Chapman Glacier surge and localized elevation changes associated with active subglacial lakes. U-DEM therefore provides a new observational basis for investigating glacier dynamics and constraining transient and inverse glacier models. More broadly, the approach demonstrates how complementary satellite observations can be integrated using machine learning to generate high-spatiotemporal-resolution records of glacier surface evolution.

https://doi.org/10.5194/egusphere-2026-5963
Preprint. Discussion started: 3 November 2026
© Author(s) 2026. CC BY 4.0 License.

Appendix A: Methods

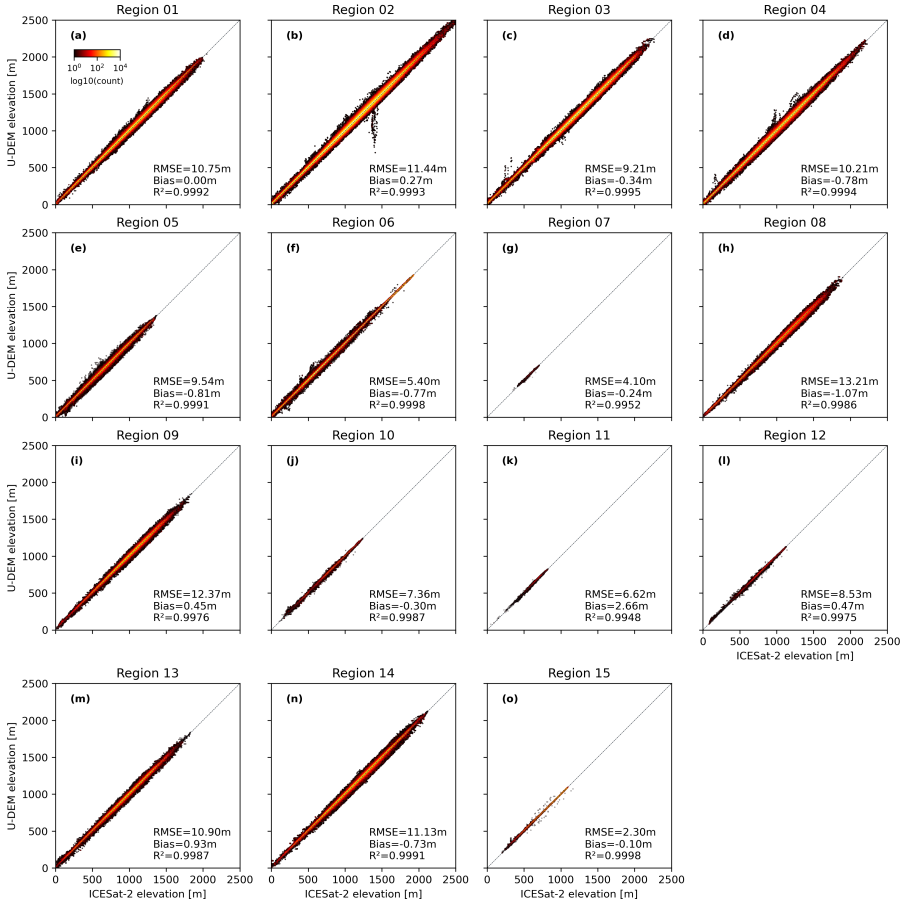


]

Figure A1. Example of how the tiles overlap and how the distance-based weight is used. This example shows how a total of 25 tiles contribute to the predictions within one tile. Dashed lines are added to tile boundaries of all tiles along the diagonals, to help distinguish the different tiles from one another.

Appendix B: Validation

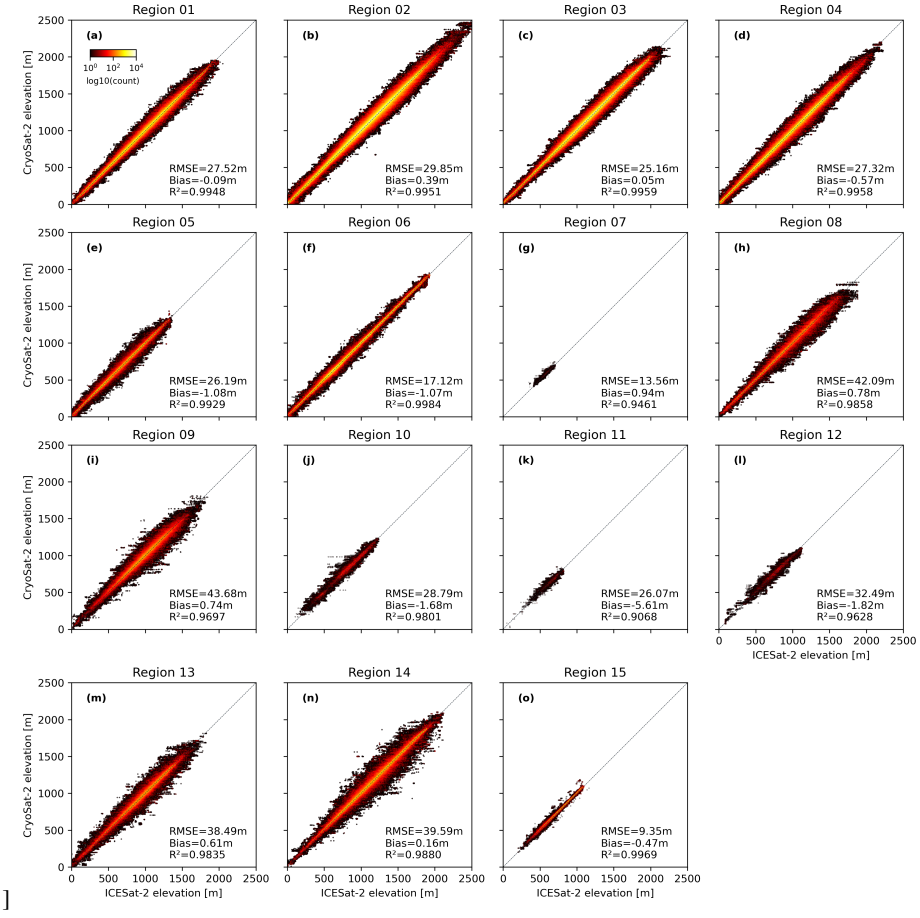
https://doi.org/10.5194/egusphere-2026-5963
Preprint. Discussion started: 3 November 2026
© Author(s) 2026. CC BY 4.0 License.



]

Figure B1. ICESat-2 elevations versus U-DEM elevations on a sub-regional basis. Regions 01-06, 12 and 15 are used in model training, whereas regions 07-11 and 13-14 are unseen by the model.

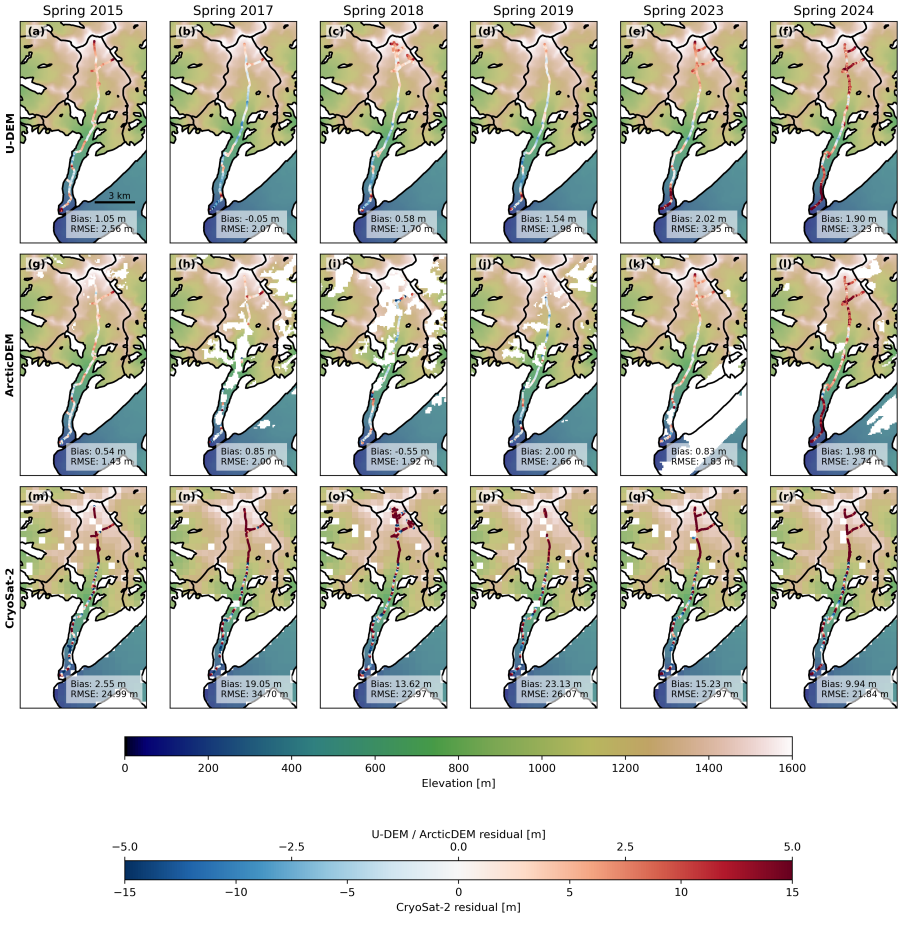
https://doi.org/10.5194/egusphere-2026-5963
Preprint. Discussion started: 3 November 2026
© Author(s) 2026. CC BY 4.0 License.



]

Figure B2. ICESat-2 elevations versus CryoSat-2 elevations on a sub-regional basis.

https://doi.org/10.5194/egusphere-2026-5963
Preprint. Discussion started: 3 November 2026
© Author(s) 2026. CC BY 4.0 License.

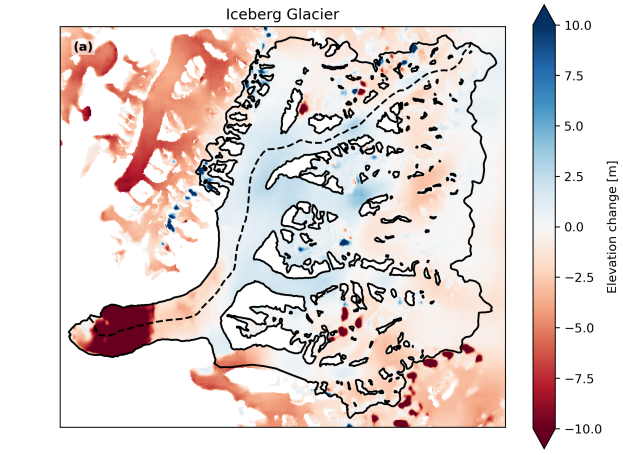


]

Figure B3. Comparison of U-DEM **(a-f)**, ArcticDEM **(g-l)** and CryoSat-2 **(m-r)** with respect to the kinematic GNSS surveys of White Glacier. Each column represent different campaign periods. Be aware that the residual colorbar for U-DEM and ArcticDEM ranges from -5 m to 5 m, whereas it ranges from -15 m to 15 m for CryoSat-2. Positive bias/residual indicate an overestimation of the surface elevation compared to the GNSS measurements.

https://doi.org/10.5194/egusphere-2026-5963
Preprint. Discussion started: 3 November 2026
© Author(s) 2026. CC BY 4.0 License.

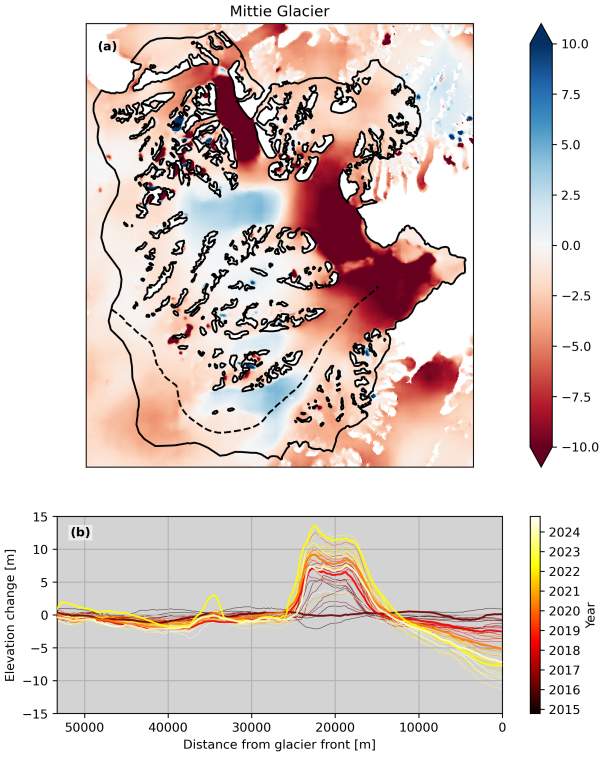
Appendix C: Applications



]

Figure C1. Quiescent phase of the surge of Iceberg Glacier, Axel Heiberg Island. **(a)** U-DEM elevation change between spring 2015 and fall 2024 of Iceberg Glacier, marked by the black outline from RGI v7 (RGI Consortium, 2023). The dashed line is the RGI v7 centerline which is plotted in panel b). **(b)** U-DEM elevation change of the centerline marked in a) with respect to spring 2015. The following springs are marked by thicker lines: 2016, 2018, 2020, 2022, 2024. Spring 2015 is the first time slice where Sentinel-1 has coverage of this region.

https://doi.org/10.5194/egusphere-2026-5963
Preprint. Discussion started: 3 November 2026
© Author(s) 2026. CC BY 4.0 License.



]

Figure C2. Quiescent phase of the surge of Mittie Glacier, Ellesmere Island. **(a)** U-DEM elevation change between fall 2014 and fall 2024 of Mittie Glacier, marked by the black outline from RGI v7 (RGI Consortium, 2023). The dashed line is the RGI v7 centerline which is plotted in panel b). **(b)** U-DEM elevation change of the centerline marked in a) with respect to fall 2014. The following springs are marked by thicker lines: 2016, 2018, 2020, 2022, 2024.

Code and data availability. The code behind U-DEM is publicly available (Zinck and Melcher, 2026a) and so are the U-DEM surface elevations and model (Zinck and Melcher, 2026b). Sentinel-1 data is available through Google Earth Engine (https://developers.google.com/earth-engine/datasets/catalog/COPERNICUS_S1_GRD, last access: 29 September 2026) and CryoSwath elevations are available from Haacker and Wouters (2025). The ArcticDEM strips and mosaic are available from the Polar Geospatial Center (https://www.pgc.umn.edu/data/arcticdem/, last access: 29 September 2026). The Randolph Glacier Inventory version 7 is available from RGI Consortium (2023) and ICESat-2 ATL06 data is available from Smith et al. (2025).

Author contributions. ASPZ designed and carried out the study with inputs from JOM and DDJ. JOM supported the model-development. LT provided GNSS data and helped interpreting the results. ASPZ lead the writing of the manuscript with inputs from all authors.

Competing interests. The authors declare no competing interests.

https://doi.org/10.5194/egusphere-2026-5963
Preprint. Discussion started: 3 November 2026
© Author(s) 2026. CC BY 4.0 License.



Acknowledgements. This research was made possible thanks to the 2022 Balzan Prize for Glaciation and Ice Sheet Dynamics awarded to Dorthe Dahl-Jensen and Johannes "Hans" Oerlemans. Data collection at White Glacier was made possible through logistical support from the Canadian Polar Continental Shelf program and through funding provided by the NSERC Discovery and Northern Supplement programs, ArcticNet, and the Canada Research Chairs program. We acknowledge coding support from ChatGPT, after which the code has been reviewed and edited as necessary. We take full responsibility for the final version of the code. JOM acknowledges funding from Independent Research Fund Denmark through the project “Arctic push on Europe’s extremes: The anatomy of Arctic impact on European climate change - ArcticPush” (Grant ID 10.46540/4258-00025B).

https://doi.org/10.5194/egusphere-2026-5963
Preprint. Discussion started: 3 November 2026
© Author(s) 2026. CC BY 4.0 License.

References

Akiba, T., Sano, S., Yanase, T., Ohta, T., and Koyama, M.: Optuna: A Next-Generation Hyperparameter Optimization Framework, https://arxiv.org/abs/1907.10902v1, 2019.

Beraud, L., Brun, F., Dehecq, A., Hugonnet, R., and Shekhar, P.: Glacier Surge Monitoring from Temporally Dense Elevation Time Series: Application to an ASTER Dataset over the Karakoram Region, The Cryosphere, 19, 5075–5094, https://doi.org/10.5194/tc-19-5075-2025, 2025.

Brangers, I., Marshall, H.-P., De Lannoy, G., Dunmire, D., Mätzler, C., and Lievens, H.: Tower-Based C-Band Radar Measurements of an Alpine Snowpack, The Cryosphere, 18, 3177–3193, https://doi.org/10.5194/tc-18-3177-2024, 2024.

Carletti, F., Marin, C., Ghielmini, C., Bavay, M., and Lehning, M.: Multitemporal Analysis of Sentinel-1 Backscatter during Snowmelt Using High-Resolution Field Measurements and Radiative Transfer Modelling, The Cryosphere, 19, 5579–5612, https://doi.org/10.5194/tc-19-5579-2025, 2025.

Cheng, Q., Zhang, Z., Liang, D., and Ye, F.: Fine Spatial and Temporal Ice/Snow Surface Temperature Generation: Evaluation Spatiotemporal Fusion Methods in Greenland Ice Sheet, IEEE Journal of Selected Topics in Applied Earth Observations and Remote Sensing, 16, 10 216–10 229, https://doi.org/10.1109/JSTARS.2023.3323742, 2023.

Cook, A. J., Copland, L., Noël, B. P. Y., Stokes, C. R., Bentley, M. J., Sharp, M. J., Bingham, R. G., and van den Broeke, M. R.: Atmospheric Forcing of Rapid Marine-Terminating Glacier Retreat in the Canadian Arctic Archipelago, Science Advances, 5, eaau8507, https://doi.org/10.1126/sciadv.aau8507, 2019.

Copland, L., Hallé, D., Wychen, W. V., Lauzon, B., Dowdeswell, J. A., and Davis, J.: Characteristics of the 15-Year Surge of Mittie Glacier, SE Ellesmere Island, Canadian Arctic, Annals of Glaciology, 65, e30, https://doi.org/10.1017/aog.2024.31, 2024.

Dai, C. and Howat, I. M.: Measuring Lava Flows With ArcticDEM: Application to the 2012–2013 Eruption of Tolbachik, Kamchatka, Geophysical Research Letters, 44, 12,133–12,140, https://doi.org/10.1002/2017GL075920, 2017.

Davison, B. J., Hogg, A. E., Gourmelen, N., Jakob, L., Wuite, J., Nagler, T., Greene, C. A., Andreasen, J., and Engdahl, M. E.: Annual Mass Budget of Antarctic Ice Shelves from 1997 to 2021, Science Advances, 9, eadi0186, https://doi.org/10.1126/sciadv.adi0186, 2023.

de Roda Husman, S., Lhermitte, S., Bolibar, J., Izeboud, M., Hu, Z., Shukla, S., van der Meer, M., Long, D., and Wouters, B.: A High-Resolution Record of Surface Melt on Antarctic Ice Shelves Using Multi-Source Remote Sensing Data and Deep Learning, Remote Sensing of Environment, 301, 113 950, https://doi.org/10.1016/j.rse.2023.113950, 2024.

Dussaillant, I., Hugonnet, R., Huss, M., Berthier, E., Bannwart, J., Paul, F., and Zemp, M.: Annual Mass Change of the World's Glaciers from 1976 to 2024 by Temporal Downscaling of Satellite Data with in Situ Observations, Earth System Science Data, 17, 1977–2006, https://doi.org/10.5194/essd-17-1977-2025, 2025.

Gorelick, N., Hancher, M., Dixon, M., Ilyushchenko, S., Thau, D., and Moore, R.: Google Earth Engine: Planetary-Scale Geospatial Analysis for Everyone, Remote Sensing of Environment, 202, 18–27, https://doi.org/10.1016/j.rse.2017.06.031, 2017.

Gourmelen, N., Escorihuela, M. J., Shepherd, A., Foresta, L., Muir, A., Garcia-Mondéjar, A., Roca, M., Baker, S. G., and Drinkwater, M. R.: CryoSat-2 Swath Interferometric Altimetry for Mapping Ice Elevation and Elevation Change, Advances in Space Research, 62, 1226–1242, https://doi.org/10.1016/j.asr.2017.11.014, 2018.

Haacker, J. and Wouters, B.: Glacier Surface Elevation Change Rate Dataset Accompanying the Article "CryoSwath: A CryoSat-2 Swath Processor and Monthly Surface Elevation Dataset for Arctic Mountain Glaciers", https://data.4tu.nl/datasets/85738a14-6652-4e0c-8552-d6fc729141b3/4, https://doi.org/10.4121/85738a14-6652-4e0c-8552-d6fc729141b3.v4, 2025.

https://doi.org/10.5194/egusphere-2026-5963
Preprint. Discussion started: 3 November 2026
© Author(s) 2026. CC BY 4.0 License.

Haacker, J., Wouters, B., and Slobbe, C.: Systematic Errors Observed in CryoSat-2 Elevation Swaths on Mountain Glaciers and Their Implications, IEEE Transactions on Geoscience and Remote Sensing, 61, 1–12, https://doi.org/10.1109/TGRS.2023.3277277, 2023.

Haacker, J., Wouters, B., Fettweis, X., Glissenaar, I. A., and Box, J. E.: Atmospheric-River-Induced Foehn Events Drain Glaciers on Novaya Zemlya, Nature Communications, 15, 7021, https://doi.org/10.1038/s41467-024-51404-8, 2024.

Hugonnet, R., McNabb, R., Berthier, E., Menounos, B., Nuth, C., Girod, L., Farinotti, D., Huss, M., Dussaillant, I., Brun, F., and Kääb, A.: Accelerated Global Glacier Mass Loss in the Early Twenty-First Century, Nature, 592, 726–731, https://doi.org/10.1038/s41586-021-03436-z, 2021.

Kern, M., Cullen, R., Berruti, B., Bouffard, J., Casal, T., Drinkwater, M. R., Gabriele, A., Lecuyot, A., Ludwig, M., Midthassel, R., Navas Traver, I., Parrinello, T., Ressler, G., Andersson, E., Martin-Puig, C., Andersen, O., Bartsch, A., Farrell, S., Fleury, S., Gascoin, S., Guillot, A., Humbert, A., Rinne, E., Shepherd, A., van den Broeke, M. R., and Yackel, J.: The Copernicus Polar Ice and Snow Topography Altimeter (CRISTAL) High-Priority Candidate Mission, The Cryosphere, 14, 2235–2251, https://doi.org/10.5194/tc-14-2235-2020, 2020.

Kingma, D. P. and Ba, J.: Adam: A Method for Stochastic Optimization, https://doi.org/10.48550/arXiv.1412.6980, 2017.

Lauzon, B., Copland, L., Wychen, W. V., Kochtitzky, W., McNabb, R., and Dahl-Jensen, D.: Dynamics throughout a Complete Surge of Iceberg Glacier on Western Axel Heiberg Island, Canadian High Arctic, Journal of Glaciology, 69, 1333–1350, https://doi.org/10.1017/jog.2023.20, 2023.

Liang, Q., Xiao, W., Howat, I., Cheng, X., Hui, F., Chen, Z., Jiang, M., and Zheng, L.: Filling and Drainage of a Subglacial Lake beneath the Flade Isblink Ice Cap, Northeast Greenland, The Cryosphere, 16, 2671–2681, https://doi.org/10.5194/tc-16-2671-2022, 2022.

Lilien, D. A., Nymand, N. F., Gerber, T. A., Steinhage, D., Jansen, D., Thomson, L., Myers, M., Franke, S., Taylor, D., Gogineni, P., Lemes, M., Vinther, B. M., and Dahl-Jensen, D.: Potential to Recover a Record of Holocene Climate and Sea Ice from Müller Ice Cap, Canada, Journal of Glaciology, 70, e72, https://doi.org/10.1017/jog.2024.75, 2024.

Mohajerani, Y., Jeong, S., Scheuchl, B., Velicogna, I., Rignot, E., and Milillo, P.: Automatic Delineation of Glacier Grounding Lines in Differential Interferometric Synthetic-Aperture Radar Data Using Deep Learning, Scientific Reports, 11, 4992, https://doi.org/10.1038/s41598-021-84309-3, 2021.

Noh, M.-J. and Howat, I. M.: Automated Stereo-Photogrammetric DEM Generation at High Latitudes: Surface Extraction with TIN-Based Search-Space Minimization (SETSM) Validation and Demonstration over Glaciated Regions, GIScience & Remote Sensing, 52, 198–217, https://doi.org/10.1080/15481603.2015.1008621, 2015.

Oktay, O., Schlemper, J., Folgoc, L. L., Lee, M., Heinrich, M., Misawa, K., Mori, K., McDonagh, S., Hammerla, N. Y., Kainz, B., Glocker, B., and Rueckert, D.: Attention U-Net: Learning Where to Look for the Pancreas, https://doi.org/10.48550/arXiv.1804.03999, 2018.

Pfeffer, W. T., Arendt, A. A., Bliss, A., Bolch, T., Cogley, J. G., Gardner, A. S., Hagen, J.-O., Hock, R., Kaser, G., Kienholz, C., Miles, E. S., Moholdt, G., Mölg, N., Paul, F., Radić, V., Rastner, P., Raup, B. H., Rich, J., Sharp, M. J., and Consortium, T. R.: The Randolph Glacier Inventory: A Globally Complete Inventory of Glaciers, Journal of Glaciology, 60, 537–552, https://doi.org/10.3189/2014JoG13J176, 2014.

Porter, C., Howat, I., Noh, M.-J., Husby, E., Khuvis, S., Danish, E., Tomko, K., Gardiner, J., Negrete, A., Yadav, B., Klassen, J., Kelleher, C., Cloutier, M., Bakker, J., Enos, J., Arnold, G., Bauer, G., and Morin, P.: ArcticDEM - Strips, Version 4.1, https://doi.org/10.7910/DVN/C98DVS, 2022.

Porter, C., Howat, I., Noh, M.-J., Husby, E., Khuvis, S., Danish, E., Tomko, K., Gardiner, J., Negrete, A., Yadav, B., Klassen, J., Kelleher, C., Cloutier, M., Bakker, J., Enos, J., Arnold, G., Bauer, G., and Morin, P.: ArcticDEM - Mosaics, Version 4.1, https://doi.org/10.7910/DVN/3VDC4W, 2023.

https://doi.org/10.5194/egusphere-2026-5963
Preprint. Discussion started: 3 November 2026
© Author(s) 2026. CC BY 4.0 License.



Radhakrishnan, K., Scott, K. A., and Clausi, D. A.: Sea Ice Concentration Estimation: Using Passive Microwave and SAR Data With a U-Net and Curriculum Learning, IEEE Journal of Selected Topics in Applied Earth Observations and Remote Sensing, 14, 5339–5351, https://doi.org/10.1109/JSTARS.2021.3076109, 2021.

RGI Consortium: Randolph Glacier Inventory - A Dataset of Global Glacier Outlines, Version 7, https://doi.org/10.5067/F6JMOVY5NAVZ, 2023.

Ronneberger, O., Fischer, P., and Brox, T.: U-Net: Convolutional Networks for Biomedical Image Segmentation, in: Medical Image Computing and Computer-Assisted Intervention – MICCAI 2015, edited by Navab, N., Hornegger, J., Wells, W. M., and Frangi, A. F., pp. 234–241, Springer International Publishing, Cham, ISBN 978-3-319-24574-4, https://doi.org/10.1007/978-3-319-24574-4_28, 2015.

Shean, D. E., Joughin, I. R., Dutrieux, P., Smith, B. E., and Berthier, E.: Ice Shelf Basal Melt Rates from a High-Resolution Digital Elevation Model (DEM) Record for Pine Island Glacier, Antarctica, The Cryosphere, 13, 2633–2656, https://doi.org/10.5194/tc-13-2633-2019, 2019.

Slater, T., Shepherd, A., Mcmillan, M., Armitage, T. W. K., Otosaka, I., and Arthern, R. J.: Compensating Changes in the Penetration Depth of Pulse-Limited Radar Altimetry Over the Greenland Ice Sheet, IEEE Transactions on Geoscience and Remote Sensing, 57, 9633–9642, https://doi.org/10.1109/TGRS.2019.2928232, 2019.

Slater, T., Shepherd, A., McMillan, M., Leeson, A., Gilbert, L., Muir, A., Munneke, P. K., Noël, B., Fettweis, X., van den Broeke, M., and Briggs, K.: Increased Variability in Greenland Ice Sheet Runoff from Satellite Observations, Nature Communications, 12, 6069, https://doi.org/10.1038/s41467-021-26229-4, 2021.

Smith, B., Adusumilli, S., Csath??, B., Felikson, D., Fricker, H., Gardner, A., Holschuh, N., Lee, J., Nilsson, J., Paolo, F., Siegfried, M., Sutterley, T., and the ICESat-2 Science Team: ATLAS/ICESat-2 L3A Land Ice Height, Version 7, https://doi.org/10.5067/ATLAS/ATL06.007, 2025.

Uhrig, J., Schneider, N., Schneider, L., Franke, U., Brox, T., and Geiger, A.: Sparsity Invariant CNNs, in: IEEE International Conference on 3D Vision (3DV), https://doi.org/10.48550/arXiv.1708.06500, 2017.

Van Wychen, W., Jiskoot, H., Shannon, K., and Gorwill, C.: The Long Multiphase Trunk–Tributary Surge History of the High-Arctic Chapman Glacier, 1959–2023, Arctic, Antarctic, and Alpine Research, 57, 2441 541, https://doi.org/10.1080/15230430.2024.2441541, 2025.

Williamson, S. N., Copland, L., Thomson, L., and Burgess, D.: Comparing Simple Albedo Scaling Methods for Estimating Arctic Glacier Mass Balance, Remote Sensing of Environment, 246, 111 858, https://doi.org/10.1016/j.rse.2020.111858, 2020.

Winstrup, M., Ranndal, H., Hillerup Larsen, S., Simonsen, S. B., Mankoff, K. D., Fausto, R. S., and Sandberg Sørensen, L.: PRODEM: An Annual Series of Summer DEMs (2019 through 2022) of the Marginal Areas of the Greenland Ice Sheet, Earth System Science Data, 16, 5405–5428, https://doi.org/10.5194/essd-16-5405-2024, 2024.

Xia, M., Li, R., Scaioni, M., An, L., Li, Z., and Qiao, G.: Building Multi-Satellite DEM Time Series for Insight into Mélange inside Large Rifts in Antarctica, The Cryosphere, 19, 6749–6770, https://doi.org/10.5194/tc-19-6749-2025, 2025.

Zheng, W., Van Wychen, W., Li, T., and Yamanokuchi, T.: Active Subglacial Lakes in the Canadian Arctic Identified by Multi-Annual Ice Elevation Changes, The Cryosphere, 20, 1699–1714, https://doi.org/10.5194/tc-20-1699-2026, 2026.

Zinck, A.-S. P. and Melcher, J. O.: Aszinck/Udem: UDEM v1.0.0, https://doi.org/10.5281/zenodo.23034293, 2026a.

Zinck, A.-S. P. and Melcher, J. O.: Dataset Belonging to the Article: "U-DEM: High Spatiotemporal Resolution Surface Elevations of the Canadian Arctic", https://doi.org/10.5281/zenodo.22657465, 2026b.

https://doi.org/10.5194/egusphere-2026-5963
Preprint. Discussion started: 3 November 2026
© Author(s) 2026. CC BY 4.0 License.



Zinck, A.-S. P., Wouters, B., Lambert, E., and Lhermitte, S.: Unveiling Spatial Variability within the Dotson Melt Channel through High-Resolution Basal Melt Rates from the Reference Elevation Model of Antarctica, The Cryosphere, 17, 3785–3801, https://doi.org/10.5194/tc-17-3785-2023, 2023.

Zinck, A.-S. P., Lhermitte, S., Wearing, M. G., and Wouters, B.: Channelized Melt beneath Antarctic Ice Shelves Previously Underestimated, Nature Climate Change, 16, 350–353, https://doi.org/10.1038/s41558-025-02537-1, 2026.